IOPscience iopscience.iop.org

Home Search Collections Journals About Contact us My IOPscience

Investigation of the Galvanic Effect between RuN Barriers and Cu Seed Layers

This content has been downloaded from IOPscience. Please scroll down to see the full text.

2011 Jpn. J. Appl. Phys. 50 121803

(http://iopscience.iop.org/1347-4065/50/12R/121803)

View the table of contents for this issue, or go to the journal homepage for more

Download details:

IP Address: 140.113.38.11
This content was downloaded on 28/04/2014 at 22:45

Please note that terms and conditions apply.

DOI: 10.1143/JJAP.50.121803

Investigation of the Galvanic Effect between RuN Barriers and Cu Seed Layers

Chia-Yang Wu, Wen-Hsi Lee, Shih-Chieh Chang[1], and Ying-Lang Wang[1]*

Department of Electrical Engineering, National Cheng Kung University, Tainan 701, Taiwan, R.O.C.
[1] *Institute of Lighting and Energy Photonics, National Chiao Tung University, Hsinchu 30050, Taiwan, R.O.C.*

Received April 22, 2011; revised August 26, 2011; accepted September 4, 2011; published online November 24, 2011

In this study, we investigated the galvanic effect between the Cu metals and ruthenium nitride (RuN_x) films that were deposited at various nitrogen (N_2) gas flow rates in chemical mechanical polishing slurries. It was found that the galvanic corrosion of the RuN_x films was inhibited with increasing N_2 gas flow ratio, whereas the galvanic corrosion of the Cu seed layers was enhanced. Electrochemical impedance spectroscopy showed that the galvanic corrosion resistance of RuN_x increased and that of the ruthenium oxide layer decreased as N_2 flow ratio increased. This was because the increase in the N content in the RuN_x films inhibited the corrosion and oxidation of the Ru metals.
© 2011 The Japan Society of Applied Physics

1. Introduction

In Cu metallization, a barrier layer is necessary to prevent the Cu metal from diffusing into the dielectric layer.[1–15] Materials used as barrier layers should not only be thin enough to reduce effective metal resistance, but should also have compatible adhesion between Cu and the dielectric layers.[16–24] In addition, good step-coverage is necessary for barrier deposition to form a uniform layer along the surfaces and corners of silicon wafers. Tantalum and tantalum nitride (Ta/TaN_x) films have been widely used as diffusion barriers for Cu metallization owing to their excellent chemical and thermal stabilities, and the physical properties of TaN_x films deposited at various nitrogen (N_2) gas flow rates have been widely investigated.[25–28)]

With the decreasing feature size of microelectronic devices, the overall thickness of the Cu seed layer and barrier metal has to be reduced to achieve the Cu electroplating process. Ruthenium (Ru) has the potential to act as both the seed and barrier layers.[29,30] However, the barrier property of pure Ru for Cu diffusion is worse than that of a Ta/TaN_x film, and Cu diffusion occurs after annealing at 450 °C for 10 min in a Cu/Ru/Si structure.[31] Therefore, how to modify the Ru metal so that it can be plated directly is very important for Ru to replace Ta/TaN_x as a Cu diffusion barrier layer. Several studies have shown that ruthenium nitride (RuN_x) barrier layers have better diffusion barrier properties and thermal stability than layers of pure Ru metals.[5–8] The N content of the RuN_x films also affects their barrier properties and thermal stability. In addition to physical properties, the chemical behavior of the RuN_x films in the chemical mechanical polishing (CMP) process should be considered to achieve a robust production line. During the CMP process, various defects are usually generated on the Cu lines because Cu metal is soft and easily corroded. Defects generated by chemical corrosion, galvanic corrosion, and photocorrosion have been examined in previous studies.[8–10] The galvanic effect is due to the difference in the electrochemical potential at the interface between the barrier and Cu in a slurry environment. Kondo *et al.* investigated the galvanic effect of metals such as tungsten (W), titanium, Ta, and their nitrides,[8] Ernur *et al.* studied the effect of slurry composition on galvanic corrosion,[9] and Tai *et al.* investigated the extent of galvanic corrosion between Cu and different barrier materials.[10] Moreover, the degree of galvanic corrosion between Cu and various barrier materials including their nitrides has been widely investigated. For example, Hung *et al.* reported that the galvanic corrosion of the TaN_x films to Cu seed layers is retarded by N.[32,33] However, to date there have been few studies about the galvanic effect between the RuN_x films and Cu seed layers. To address this gap in the literature, in the present study, we investigate the galvanic effect between Cu seed layers and RuN_x films deposited at various N_2 gas flow rates in CMP slurries by electrochemical impedance spectroscopy (EIS),[34–39] energy dispersive X-ray (EDX), and field-emission scanning electron microscopy (FESEM).

2. Experimental Procedure

Blanket wafers were deposited with 200-nm-thick Cu seed layers using the ionized metal plasma (IMP) process on Si(100) substrates. In IMP deposition, inductively coupled Ar/N_2 plasma was used to ionize sputtered atoms. The RuN_x barriers were deposited by direct-current (DC) magnetron sputtering at 10 W forward power from a Ru target (99.99%). The Ar flow rate was kept at 20 sccm, and the nitrogen flow rate was varied from 0 to 20 sccm, resulting in a process pressure of $\sim$0.1 Torr. The nitrogen flow ratios $[N_2/(Ar + N_2)]$ were (1) 0, (2) 20, (3) 33, (4) 43, and (5) 50%. The gas purity was 99.9999% and the gas flow rate was controlled within $\pm$0.1 sccm by mass flow controllers, which guaranteed repeatability. After the RuN_x film deposition, a 200-nm-thick Cu seed layer was then deposited. In the corrosion analyses, the RuN_x films deposited at various N_2 flow ratios were used as the working electrodes (1 cm^2), the Cu seed layers were used as the counterelectrodes (1 cm^2), and Ag/AgCl was used as the reference electrode in a Cu CMP slurry, which contained aluminum oxide abrasive, surfactant, and hydrogen peroxide (5% H_2O_2) with a pH in the range of 6–7. In this case, impedance was not measured until open circuit potential (OCP) became stable, which could minimize the inaccuracies in the experiment. The potential difference was measured by electrically connecting the working electrode and the reference electrode to an electrometer, which is a high-impedance multimeter that can measure voltage, resistance, and current. The potential difference between the Cu seed layers and the RuN_x films was obtained by subtracting the two potential differences measured using the Cu and RuN_x electrodes with respect to the Ag/AgCl reference electrode. The measurement was not

*E-mail address: ylwang@tsmc.com

© 2011 The Japan Society of Applied Physics

conducted by connecting the the two electrodes directly. The N content of the RuN_x films was determined using an X-ray photoelectron spectrometer (XPS) and the O ratio of RuN_x films after 90 s immersion in the slurry was determined by EDX. The electron binding energy of Ru was measured by XPS and the stoichiometric composition of the RuN films was measured by XPS. In addition, the cross-sectional profile and the thickness of the RuN_x and Cu films before and after immersion in the slurry were obtained by FESEM (KLA-Tencor SEMVision). EIS is widely recognized as a powerful tool for the investigation of electrochemical behaviors,[34–39] and thus it was used to characterize the galvanic corrosion between the RuN_x films and the Cu seed layers. Therefore, the RuN films were used as the working electrode and the Cu film as the counterelectrode. The OCP between the deposited RuN_x film (1 cm^2) and a platinum plate (1 cm^2) was examined using a Princeton Applied Research PARSTAT 2273. The Nyquist plot was also obtained using a PARSTAT 2273 and the alternating current (AC) impedance behavior of the capacitor cells was analyzed. The impedance measurements were carried out at various potentials with a DC potential of 0 mV associated with OCP and a frequency range from 100 mHz to 400 kHz. The equivalent circuit was built up and simulated using software ZSimpWin version 3.1 with EIS data.

3. Results and Discussion

Figures 1(a)–1(c) show the microstructures of RuN_x films in which the nitrogen content varied from 0 to 50%. The microstructures of the RuN_x films were examined by SEM. It was found that pure Ru has a column structure. In the presence of nitrogen, the grain size decreased, the number of defects increased, and the structure transformed into RuN_x. The composition of the RuN films was also measured by XPS. As shown in Table I, the N content of the RuN films increased significantly with N_2 flow ratio.

The potential dynamic curves were used to determine the corrosion effect between the Cu seed layers and the RuN_x films, as shown in Fig. 2. It can be seen that the corrosion current densities of the Cu seed layers were slightly higher than those of the RuN_x films, which implies that the intrinsic corrosion rates of the Cu seed layers were higher than those of the RuN_x films. In addition, Fig. 3 shows that the OCP of the Cu seed layers was more negative than those of the RuN_x films, which also indicates that the RuN_x films were nobler than the Cu seed layers with regard to their activity in the slurry. (Note that each OCP was first compared with that of the Ag/AgCl reference electrode in OCP measurement.) We then obtained the potential difference between the Cu seed layers and RuN_x films by subtracting the OCP measured in the previous OCP measurement.

In the electrochemical analysis, negative OCPs indicate that the Cu seed layers were the substrate that was more easily corroded. For RuN_x films, the OCP became more positive with increasing nitrogen content, indicating that RuN_x films with N doping were less corroded. This suggests that increasing the N content in RuN_x films suppresses electron release owing to the high electronegativity of N atoms. Figure 4 shows that the binding energy of the Ru peaks ($3d_{3/2}$: 284.2 eV, $3d_{5/2}$: 280.0 eV) was split, and some of these peaks shifted slightly to a higher value. This phenomenon is

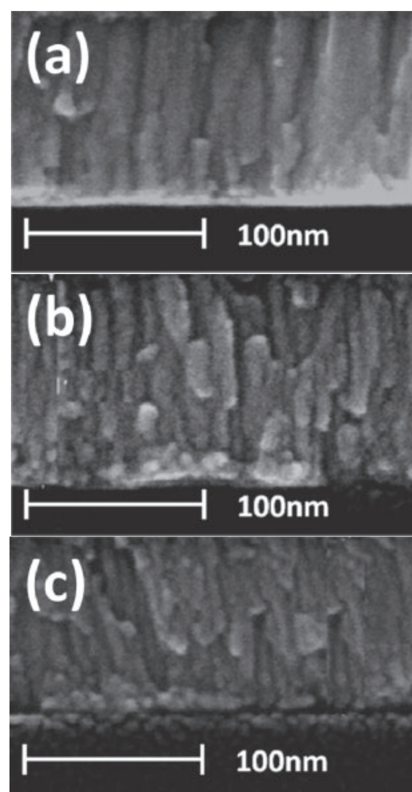

Fig. 1. SEM cross-sectional images before slurry dipping of RuN_x films deposited at N_2 gas flow ratios of (a) 0, (b) 20, and (c) 50%.

Table I. Atomic ratio of Ru and RuN films.

Sputtering nitrogen ratio $[N_2/(N_2 + Ar)]$ (%)	Ru atomic ratio (%)	N atomic ratio (%)
0	99.6	0.4
20	93.3	6.7
33	91.0	9.0
43	86.5	13.5
50	77.6	22.4

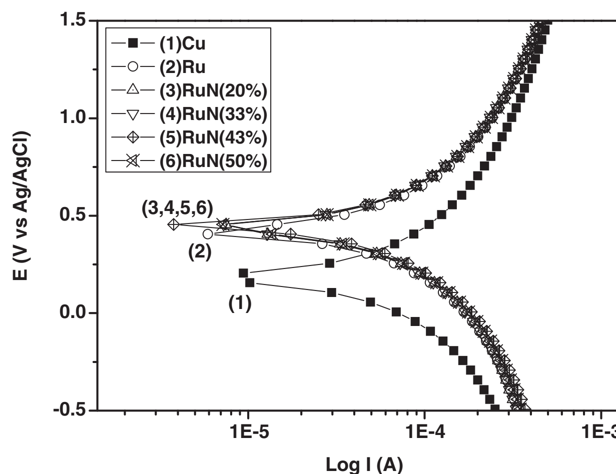

Fig. 2. Potential dynamic curves of the Cu seed layer and the RuN_x films deposited at various N_2 gas flow ratios in the slurries.

© 2011 The Japan Society of Applied Physics

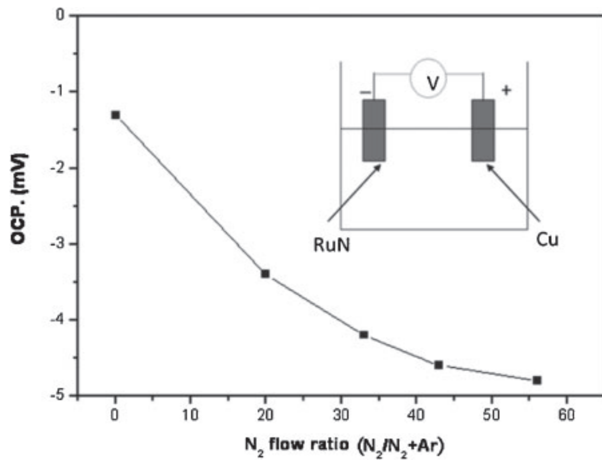

Fig. 3. Potential difference between the Cu seed layers and RuN_x films measured with an electrometer.

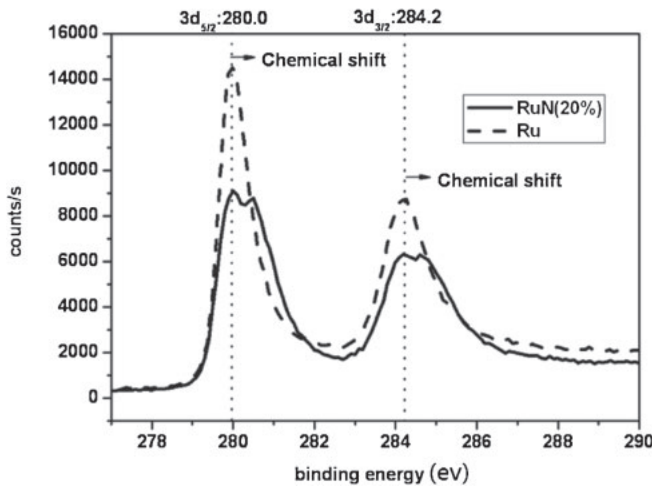

Fig. 4. XPS spectra of the as-deposited pure Ru and RuN films.

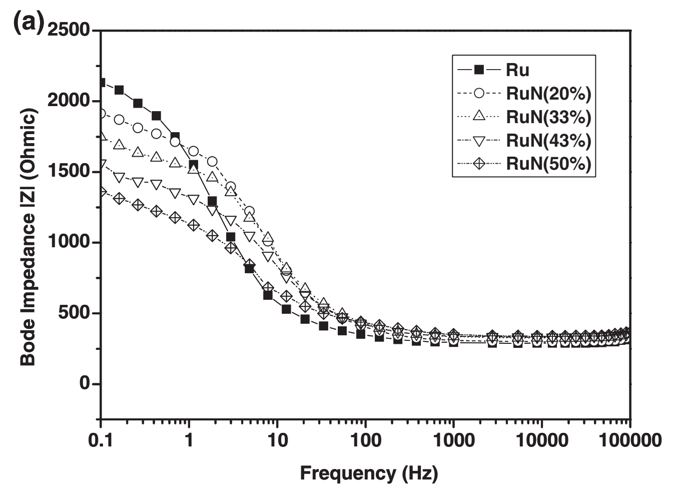

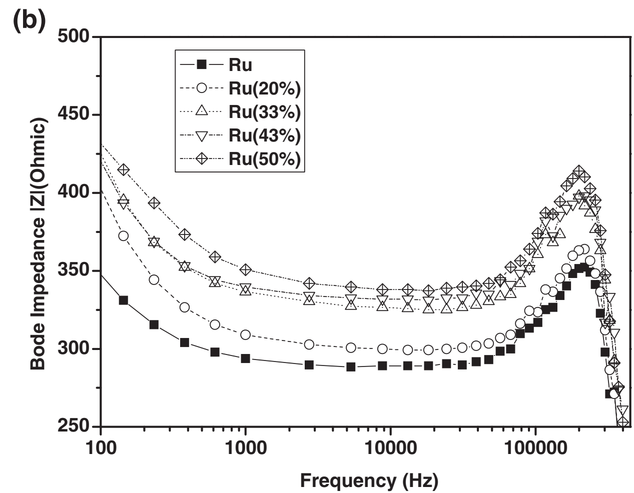

Fig. 5. (a) Bode plots of the Cu–RuN electrochemical system in the CMP slurry with the RuN_x films deposited at N_2 gas flow ratios from 0 to 50%, and (b) magnification of the high-frequency region.

due to the fact that the electrons in the Ru atoms were in different valence states, inducing the chemical shift. The increase in binding energy indicates that N in the RuN_x films suppresses electron release and inhibits oxidation.

The galvanic corrosion rate of RuN_x films is lower than the self-corrosion rate, indicating that the corrosion rate of RuN_x films is decreased by the galvanic effect. In contrast, the galvanic corrosion rate of Cu is larger than the self-corrosion rate. The Bode plots in Fig. 5(a) show the effect of applied frequency on the impedance between the Cu seed layers and the RuN_x films deposited at N_2 gas flow ratios from 0 to 50%. In this case, the RuN_x films deposited at various N_2 flow rates were used as the working electrodes, the Cu films were used as the counterelectrodes, and all potentials were measured relative to that of the Ag/AgCl reference electrode. In the low-frequency region (0.1–1 Hz), the impedance decreased with increasing N_2 content. In contrast, the impedance slightly increased with increasing N_2 content in the high-frequency region (>100 kHz), as shown in Fig. 5(b).

Figure 6 shows the Nyquist plots of the Cu–RuN_x electrochemical system in the CMP slurry. The Nyquist plots in Fig. 6(b) also show that $Z_{\rm im}$ and $Z_{\rm re}$ both increased with increasing N_2 content in the high-frequency (20–400 kHz) region, which means that the RuN_x films doped with a high N content were less corroded. Figure 6(a) shows the Cu–RuN_x system measured from the middle-frequency region to the low-frequency region. The Nyquist plots of the Cu–RuN_x electrochemical system can be fitted with two semicircles using ZSimpWin: a small semicircle in the high-frequency range (>20 Hz) followed by a large semicircle in the middle-low-frequency range (<20 Hz). The second semicircle reveals that both $Z_{\rm im}$ and $Z_{\rm re}$ decrease with increasing N_2 content in the low-frequency (0.1–20 Hz) region, indicating that the Ru films oxidize more easily than the RuN_x films.

Figure 7 shows the simulated equivalent circuit of the Cu–RuN_x electrochemical system. In this circuit, the series and parallel combinations of resistance or capacitance elements indicate whether their representative reactions occur sequentially (in series) or simultaneously (in parallel).[40] $R_{\rm s}$ is the bulk-solution resistance, $C_{\rm dl}$ is the double-layer capacitance of the electrogenerated from the surface corrosion of the RuN_x films, and $R_{\rm corr}$ is the corrosion resistance (associated with the double layer). The chemical reaction of the RuN_x films in the Cu–RuN_x electrochemical system occurs through the following intermediate steps:

 © 2011 The Japan Society of Applied Physics

Table II. Element values of equivalent circuit in Fig. 6 required for the best fitting of impedance spectra in Fig. 5.

	R_s (Ω)	R_{corr} (Ω)	CPE_{dl}			R_{ox} (Ω)	CPE_{ox}		
			Q	n	C_{dl} (pF)		Q	n	C_{ox} (mF)
RuN (0%)	21	260	4.00×10^{-12}	0.952	1.41	1982	2.01×10^{-9}	0.750	0.0583
RuN (20%)	17	275	4.50×10^{-12}	0.946	1.40	1678	2.00×10^{-9}	0.720	0.0257
RuN (33%)	25	289	3.80×10^{-12}	0.951	1.31	1486	1.88×10^{-9}	0.710	0.0245
RuN (43%)	22	305	4.22×10^{-12}	0.944	1.25	1165	1.71×10^{-9}	0.725	0.0239
RuN (50%)	21	310	4.15×10^{-12}	0.942	1.18	864	1.73×10^{-9}	0.710	0.0196

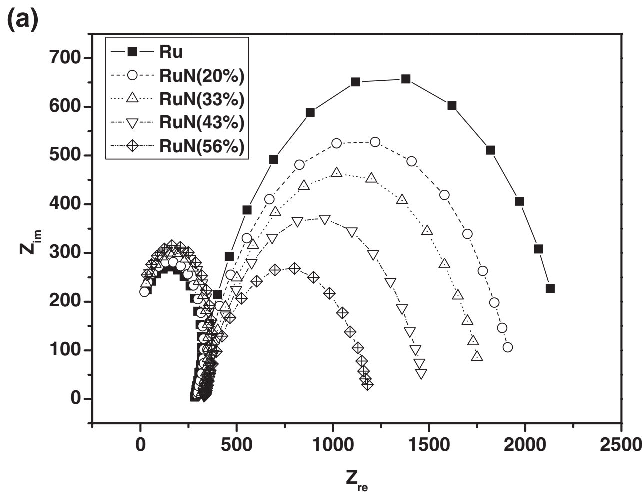

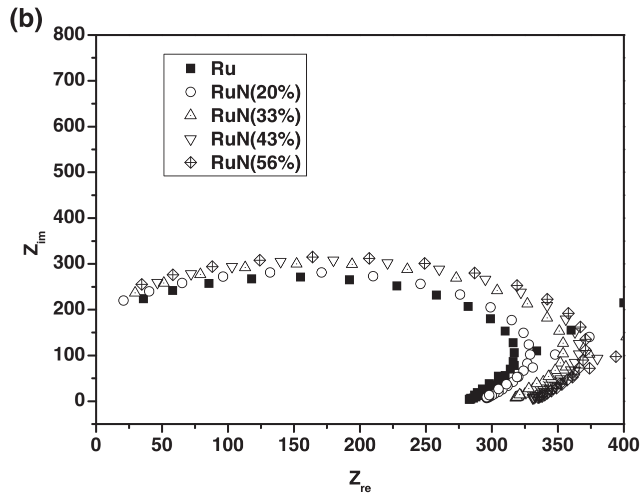

Fig. 6. (a) Nyquist plots of the Cu–RuN electrochemical system in the CMP slurry with the RuN_x films deposited at N_2 gas flow ratios from 0 to 50%, and (b) magnification of impedance close to zero in the high-frequency region.

$$Ru \rightarrow Ru^{4+} + 4e^- \tag{1}$$

$$Ru^{4+} + 2O^{2-} \rightarrow RuO_2. \tag{2}$$

In eq. (2), C_{ox} is the capacitance of the RuN_x oxidization layer, and R_{ox} is the resistance of the RuN_x oxidization layer. On the other hand, the two semicircles shown in Fig. 5 indicate the transient surface oxidation of the RuN_x films. The first semicircle (high-frequency region) indicates the continuous corrosion of the RuN_x films, and the second semicircle (middle-low-frequency region) indicates the Ru metal oxides in the peroxide-based solutions.

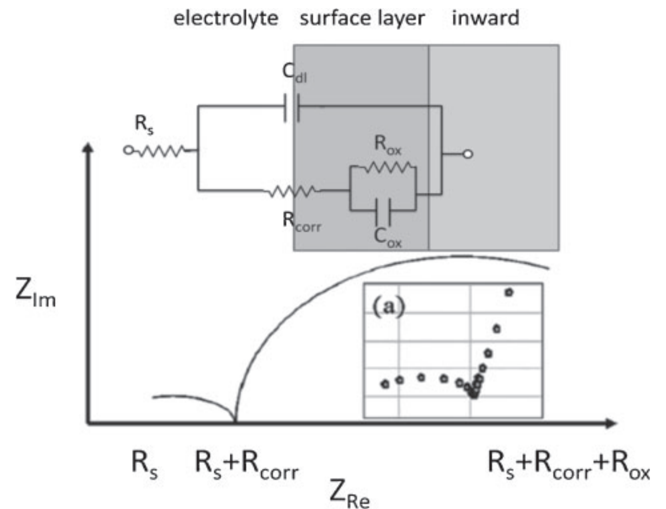

Fig. 7. Proposed equivalent circuit diagram showing the electrochemical characteristics of RuN_x galvanic corrosion in the CMP slurry solution, where R_s is the bulk-solution resistance, C_{dl} is the double-layer capacitance, R_{corr} is the corrosion resistance (associated with the double layer), C_{ox} is the oxidization-layer capacitance, and R_{ox} is the oxidization resistance of RuN_x.

The values of each component in the circuit of Fig. 7 are obtained by fitting the Nyquist spectra in Fig. 6, and they are summarized in Table II, where CPE_{dl} is the impedance of the constant phase element (CPE) of the electrogenerated double layer from surface corrosion of the RuN_x films, and CPE_{ox} is the impedance of the RuN_x oxidation layer. The capacitances in the system can be transferred from CPE using[41–43]

$$C_{dl} = \frac{(Q_{dl} \times R_{corr})^{(1/n)}}{R_{corr}}, \tag{3}$$

$$C_{ox} = \frac{(Q_{ox} \times R_{ox})^{(1/n)}}{R_{ox}}. \tag{4}$$

Consequently, R_{corr} increases with the increase in N_2 content, while R_{ox} decreases, as shown in Table II. This is because the RuN_x films doped with high N content are more resistant to oxidization and are less corroded than those doped at lower N content.

Figure 8 shows the oxygen content of the RuN_x films, which decreases as N_2 flow rate decreases because RuN_x film's oxidation is retarded and the double-layer capacitance of the electrogenerated double layer is restricted. This demonstrates that RuN_x films doped at high N content are more resistant to oxidization because the N element holds the electrons strongly. Therefore, increasing the N ratio in the RuN_x films decreases the galvanic corrosion rate of

© 2011 The Japan Society of Applied Physics

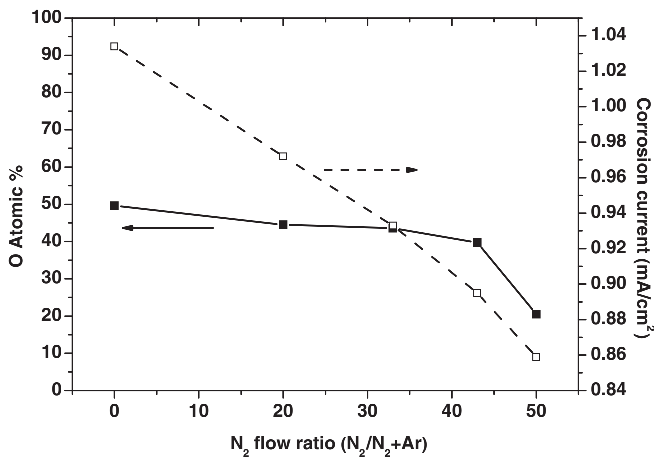

Fig. 8. Relationship for RuN_x films deposited at various N_2 gas flow rates between EDX of O element ratio after a 90 s dip and corrosion current in Cu–RuN_x system.

RuN_x and the reduction rate of the Cu seed layers. The extent of galvanic corrosion for the Cu seed layers and the RuN_x films thus depends on their potential difference. Furthermore, according to Stern and Geary,[44] and Stern[45] the following equation shows the mathematical relationship between corrosion resistance and corrosion current for polarization data.

$$I_{corr} = \frac{\beta_a \times \beta_b}{2.303 R_{corr}(\beta_a + \beta_b)}, \quad (5)$$

where I_{corr} and R_{corr} are the corrosion current and corrosion resistance, respectively, and β_a and β_b are the anodic Tafel slope and cathodic Tafel slope, respectively. According to our previous experiments, self-corrosion occurs in the TaN_x films;[31,32] it decreases with increasing N_2 flow ratio. The results of the impedance measurements and the potential differences between the Cu seed layers and the RuN_x films measured using an electrometer system show that the corrosion current decreases from 1.034 to 0.859 mA when the N_2 flow ratio for RuN_x deposition increases from 0 to 50%, as shown in Fig. 8. This result is consistent with the results of our previous investigation, which showed that the galvanic corrosion current is inhibited by the N element of TaN_x films.[31,32] The parameters in impedance spectroscopy show that a larger R_{corr} and smaller R_{ox} indicate that the RuN_x metal was more resistant to corrosion or formation of the RuO_2 layer. C_{ox} is related to the formation of RuO_2.

The proposed mechanism for the corrosion of the Cu seed layers and the RuN_x films in acidic slurry is shown in Fig. 9. For Cu films, the overall extent of corrosion is dominated by the intrinsic corrosion in the slurry. In this study, the intrinsic Cu corrosion rate was about 38.67 nm/min and the galvanic corrosion rate of the Cu films was about 111–200 nm/min, which depended on the N content of the RuN_x films, as shown in Table III. When the N_2 gas flow ratio was increased for RuN_x deposition, the galvanic corrosion of the RuN_x films was suppressed owing to the electronegativity of the N element, whereas the Cu galvanic corrosion was enhanced because the Cu metal received fewer electrons from the RuN_x film.

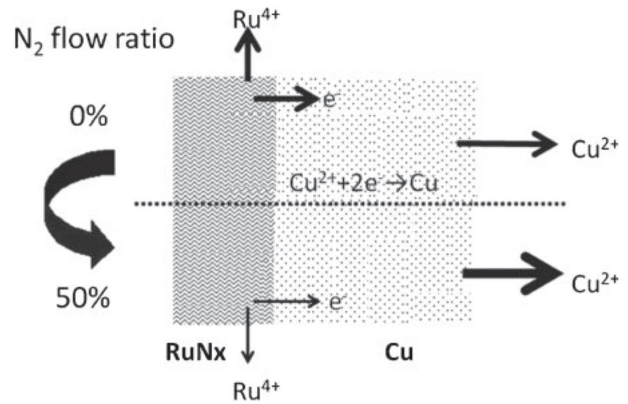

Fig. 9. Proposed mechanism of the galvanic effect between the Cu seed and the RuN_x films.

Table III. Summary of intrinsic and galvanic corrosion rates of Cu films and RuN_x films deposited at various N_2 gas flow ratios. Units are in nm/min.

N_2 flow ratio (%)	RuN_x self-corrosion rate (nm/min)	RuN_x galvanic corrosion rate (nm/min)	Cu self-corrosion rate (nm/min)	Cu galvanic corrosion rate (nm/min)
0	0.672	0.092	38.67	111.79
20	0.636	0.088	—	162.36
33	0.627	0.087	—	175.67
43	0.602	0.084	—	182.32
50	0.566	0.082	—	202.29

4. Conclusions

The purpose of this study is to investigate the galvanic effect between the Cu metals and RuN_x films. The N content of RuN_x films influenced not only the physical film properties, but also the chemical activity in the CMP process. To obtain a robust Cu metallization process, the N content of the RuN_x barriers should be optimized to achieve a compromise between the barrier properties and chemical stability. The mechanism of galvanic corrosion in the Cu–RuN_x electrochemical system was investigated, and a computer simulation using EIS data produced an equivalent circuit of the surface reaction with regard to the relationship of the RuN_x films with the Cu seed layers. The corrosion resistance increased with the N_2 flow ratio for RuN_x deposition, but the opposite results were found for the ruthenium oxide resistance associated with ruthenium oxide capacitance. This demonstrates that the N element effectively inhibits the oxidation of the Ru metals and decreases the galvanic corrosion rate of the RuN_x films. In this study, we thus conclude that increasing the N content in the RuN_x films suppresses the electron release, because the N element has high electronegativity, similarly to fluorine and oxygen. The chemical shift of the RuN_x electron shows that the N content makes RuN_x more resistant to oxidation.

Acknowledgments

This work was supported by the National Science Council of Taiwan (Grant No. NSC 99-2622-E-006-034-CC3). The authors thank National Cheng Kung University, Tainan,

© 2011 The Japan Society of Applied Physics

Taiwan, for technical support. National Cheng Kung University also assisted in meeting the publication costs of this article.

1) D. Edelstein, J. Heidenreich, R. Goldblatt, W. Cote, C. Uzoh, N. Lustig, P. Roper, T. McDevitt, W. Motsiff, A. Simon, J. Dukovic, R. Wachnik, H. Rathore, R. Schulz, L. Su, S. Luce, and J. Slattery: IEDM Tech. Dig., 1997, p. 773.
2) P. C. Andricacos, C. Uzoh, J. O. Dukovic, J. Horkans, and H. Deligianni: IBM J. Res. Dev. **42** (1998) 567.
3) K. W. Chen, Y. L. Wang, L. Chang, S. C. Chang, F. Y. Li, and S. H. Lin: Electrochem. Solid-State Lett. **7** (2004) G238.
4) A. Beverina, H. Bernard, J. Palleau, J. Torres, and F. Tardif: Electrochem. Solid-State Lett. **3** (2000) 156.
5) A. Jindal and S. V. Babu: J. Electrochem. Soc. **151** (2004) G709.
6) Y. Homma, S. Kondo, N. Sakuma, K. Hinode, J. Noguchi, N. Ohashi, H. Yamaguchi, and N. Owada: J. Electrochem. Soc. **147** (2000) 1193.
7) S. Tamilmani, W. Huang, and S. Raghavan: J. Electrochem. Soc. **153** (2006) F53.
8) S. Kondo, N. Sakuma, Y. Homma, and N. Ohashi: Jpn. J. Appl. Phys. **39** (2000) 6216.
9) D. Ernur, S. Kondo, D. Shamiryan, and K. Maex: Microelectron. Eng. **64** (2002) 117.
10) K. Tai, H. Ohtorii, S. Takahashi, N. Komai, H. Horikoshi, S. Sato, Y. Ohoka, Y. Segawa, M. Ishihara, Z. Yasuda, and T. Nogami: IEEE 2002 Int. Interconnect Technology Conf., 2002, p. 194.
11) S. C. Chang, J. M. Shieh, J. Y. Fang, Y. L. Wang, B. T. Dai, and M. S. Feng: J. Vac. Sci. Technol. B **22** (2004) 116.
12) W. T. Tseng, C. W. Liu, B. T. Dai, and C. F. Yeh: Thin Solid Films **290** (1996) 458.
13) T. Hara, F. Togoh, T. Kurosu, K. Sakamoto, Y. Shioya, T. Ishimaru, and T. K. Doy: Electrochem. Solid-State Lett. **4** (2001) G65.
14) B. Du and I. I. Suni: Electrochem. Solid-State Lett. **8** (2005) 283.
15) S. C. Kurity, S. Seal, W. Fei, J. Ramsdell, V. H. Desai, Y. Li, S. V. Babu, and B. Wood: J. Electrochem. Soc. **150** (2003) C36.
16) Y. L. Chin, B. S. Chiou, and W. F. Wu: Jpn. J. Appl. Phys. **41** (2002) 3057.
17) W. F. Wu, C. C. Wu, K. L. Ou, and C. P. Chou: J. Electrochem. Soc. **150** (2003) G83.
18) C. C. Chang, J. S. Chen, and W. S. Hsu: J. Electrochem. Soc. **151** (2004) 746.
19) A. A. Istratov and E. R. Weber: J. Electrochem. Soc. **149** (2002) G21.
20) K. M. Latt, Y. K. Lee, S. Li, T. Osipowicz, and H. L. Seng: Mater. Sci. Eng. B **84** (2001) 217.
21) E. Kolawa, J. S. Chen, J. S. Reid, P. J. Pokela, and M. A. Nicolet: J. Appl. Phys. **70** (1991) 1369.
22) W. F. Wu, K. L. Ou, C. P. Chou, and C. C. Wu: J. Electrochem. Soc. **150** (2003) G83.
23) M. Stavrev, C. Wenzel, A. Moller, and K. Drescher: Appl. Surf. Sci. **91** (1995) 257.
24) S. M. Rossnagel and H. Kim: J. Vac. Sci. Technol. B **21** (2003) 2550.
25) J. C. Lin and C. Lee: J. Electrochem. Soc. **146** (1999) 3466.
26) A. E. Kaloyeros, X. Chen, T. Stark, S. C. Seo, G. G. Peterson, H. L. Frisch, B. Arkles, and J. Sullivan: J. Electrochem. Soc. **146** (1999) 170.
27) N. D. Cuong, D.-J. Kim, B.-D. Kang, C. S. Kim, K.-M. Yu, and S.-G. Yoon: J. Electrochem. Soc. **153** (2006) G164.
28) S. C. Chang, Y. L. Wang, and T. C. Wang: IEEE Trans. Semicond. Manuf. **17** (2004) 384.
29) T. P. Moffat, M. Walker, P. J. Chen, J. E. Bonevich, W. F. Egelhoff, L. Richter, C. Witt, T. Aaltonen, M. Ritala, M. Leskelä, and D. Josella: J. Electrochem. Soc. **153** (2006) C37.
30) O. Chyan, T. N. Arunagiri, and T. Ponnuswamy: J. Electrochem. Soc. **150** (2003) C347.
31) R. Chan, T. N. Arunagiri, Y. Zhang, O. Chyan, R. M. Wallace, M. J. Kim, and T. Q. Hurdc: Electrochem. Solid-State Lett. **7** (2004) G154.
32) C. C. Hung, Y. S. Wang, W. H. Lee, S. C. Chang, and Y. L. Wang: Electrochem. Solid-State Lett. **10** (2007) H127.
33) C. C. Hung, Y. S. Wang, W. H. Lee, S. C. Chang, and Y. L. Wang: Electrochem. Solid-State Lett. **10** (2007) D100.
34) J. E. Garland, C. M. Pettit, and D. Roy: Electrochim. Acta **49** (2004) 2623.
35) M. J. Walters, J. E. Garland, C. M. Pettit, D. S. Zimmerman, D. R. Marr, and D. Roy: J. Electroanal. Chem. **499** (2001) 48.
36) C. Gabrielli: in *Physical Electrochemistry: Principles, Methods, and Applications*, ed. I. Rubinstein (Dekker, New York, 1995).
37) D. D. Macdonald: Electrochim. Acta **51** (2006) 1376.
38) V. R. K. Gorantla, K. A. Assiongbon, S. V. Babu, and D. Roy: J. Electrochem. Soc. **152** (2005) G404.
39) V. R. K. Gorantla, S. B. Emery, S. Pandija, S. V. Babu, and D. Roy: Mater. Lett. **59** (2005) 690.
40) V. R. K. Gorantla, K. A. Assiongbon, S. V. Babu, and D. Roy: J. Electrochem. Soc. **152** (2005) G404.
41) L. Larabi, O. Benali, S. M. Mekelleche, and Y. Harek: Appl. Surf. Sci. **253** (2006) 1371.
42) E. Barsoukov and J. R. Macdonald: *Handbook of Impedance Spectroscopy* (Wiley, Hoboken, NJ, 2005) p. 37.
43) M. E. Orazem, P. Shukla, and M. A. Membrino: Electrochim. Acta **47** (2002) 2027.
44) M. Stern and A. L. Geary: J. Electrochem. Soc. **104** (1957) 56.
45) M. Stern: Corrosion **14** (1958) 61.

© 2011 The Japan Society of Applied Physics